NANO LETTERS

Letter

pubs.acs.org/NanoLett

Chemical Bath Deposition of p-Type Transparent, Highly Conducting $(CuS)_x:(ZnS)_{1-x}$ Nanocomposite Thin Films and Fabrication of Si Heterojunction Solar Cells

Xiaojie Xu,[†,‡] James Bullock,[§,‡] Laura T. Schelhas,[⊥] Elias Z. Stutz,[▽,‡] Jose J. Fonseca,[∥,‡] Mark Hettick,[§,‡] Vanessa L. Pool,[⊥] Kong Fai Tai,[¶] Michael F. Toney,[⊥] Xiaosheng Fang,[†] Ali Javey,[‡,§] Lydia Helena Wong,[¶] and Joel W. Ager*[,‡,∥]

[†]Department of Materials Science, Fudan University, Shanghai 200438, P. R. China

[‡]Materials Sciences Division, Lawrence Berkeley National Laboratory, Berkeley, California 94720, United States

[§]Electrical Engineering and Computer Sciences and [∥]Materials Science and Engineering, University of California at Berkeley, Berkeley, California 94720, United States

[⊥]Stanford Synchrotron Radiation Lightsource, SLAC National Accelerator Laboratory, Menlo Park, California 94025, United States

[▽]Swiss Federal Institute of Technology (EPFL), Lausanne 1015, Switzerland

[¶]School of Materials Science and Engineering, Nanyang Technological University, Singapore 639798

Supporting Information

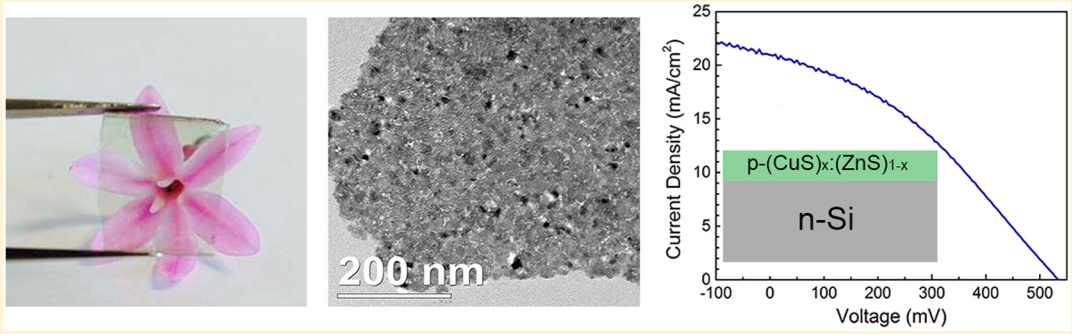

ABSTRACT: P-type transparent conducting films of nanocrystalline $(CuS)_x:(ZnS)_{1-x}$ were synthesized by facile and low-cost chemical bath deposition. Wide angle X-ray scattering (WAXS) and high resolution transmission electron microscopy (HRTEM) were used to evaluate the nanocomposite structure, which consists of sub-5 nm crystallites of sphalerite ZnS and covellite CuS. Film transparency can be controlled by tuning the size of the nanocrystallites, which is achieved by adjusting the concentration of the complexing agent during growth; optimal films have optical transmission above 70% in the visible range of the spectrum. The hole conductivity increases with the fraction of the covellite phase and can be as high as 1000 S cm^{-1}, which is higher than most reported p-type transparent materials and approaches that of n-type transparent materials such as indium tin oxide (ITO) and aluminum doped zinc oxide (AZO) synthesized at a similar temperature. Heterojunction p-$(CuS)_x:(ZnS)_{1-x}$/n-Si solar cells were fabricated with the nanocomposite film serving as a hole-selective contact. Under 1 sun illumination, an open circuit voltage of 535 mV was observed. This value compares favorably to other emerging heterojunction Si solar cells which use a low temperature process to fabricate the contact, such as single-walled carbon nanotube/Si (370−530 mV) and graphene/Si (360−552 mV).

KEYWORDS: *transparent conducting materials, p-type, chemical bath deposition, heterojunctions, photovoltaics*

Transparent conducting materials (TCMs) are widely used in electronic devices such as solar cells,[1,2] light emitting diodes (LED),[3] flat-panel displays,[4] and other optoelectronic devices.[5−7] Materials that possess both high transparency and conductivity are generally n-type (electron conducting). Examples include all of the currently commercialized TCMs such as Sn-doped In_2O_3 (ITO),[8,9] F-doped SnO_2 (FTO),[10,11] and Al-doped ZnO (AZO).[12,13] In contrast, it has been substantially more difficult to realize the combination of high hole conductivity and optical transparency required for a practical p-TCM.[14] As a result, no commericialized devices use p-TCMs; for example, efficient photovoltaic devices using p-type TCMs have yet to be demonstrated.[15]

The first p-type TCM to be reported was delafossite $CuAlO_2$ in 1997; it had a hole conductivity up to 1 S cm^{-1} and an average optical transparency of 70%.[16] Since then, considerable

Received: December 15, 2015
Revised: February 1, 2016
Published: February 8, 2016

DOI: 10.1021/acs.nanolett.5b05124
Nano Lett. 2016, 16, 1925−1932

efforts have been made to improve the performance of p-type TCMs.[17,18] For example, replacing the Al in the delafossite structure with other elements such as Ga,[19] Cr,[20] or Fe,[21] leads to films with high optical transmittance (>80% in the visible) but low conductivity (<100 S/cm), particularly when compared to typical n-type TCMs (>1000 S/cm). Many other materials systems have been investigated such as layered oxychalcogenides $(LaO)CuC^{h}$ (C^{h} = chalcogenides, e.g., S and Se),[22] spinel oxides (AB_2O_4, e.g., $NiCo_2O_4$),[23] mixed oxides (e.g., In_2O_3–Ag_2O).[24] Still, the combination of high transparency and hole-conductivity required for a technologically useful p-TCM has not been achieved.[14] It is also notable that many of the better performing p-TCMs are made with physical vapor deposition methods such as pulsed laser deposition (PLD),[25] sputtering,[26] and electron-beam evaporation[27] and also typically involve either a high growth or annealing temperature.

In this context, development of a low temperature, tunable, and scalable method for producing high performance p-TCMs is clearly desirable. In this study, we employed chemical bath deposition (CBD). This technique is facile, low-cost, and scalable, and it can deposit films on almost any substrate. It is commercially used in CdTe PV technology to deposit the electron collecting contact[28,29] and has many applications in coating technology in general.[30,31] Also, CBD usually takes place in aqueous solution at a low temperature (30–80 °C), which greatly increases the process compatibility.[32]

Kudo and co-workers reported that Cu-doped ZnS had p-type conductivity in 1999.[33] Since then, several efforts have been made to explore the Cu–Zn–S system as a p-type transparent conductor. For example, Diamond et al.[34] obtained p-type transparent copper-alloyed ZnS films by PLD at elevated temperature, with the optimal films exhibiting conductivities of 54 S cm^{-1} and optical transmission of 65% at 550 nm. Solution-based approaches have been investigated recently, as well. For example, Yang et al.[35] fabricated hole conductive Cu:ZnS films by electrochemical deposition; the optimized Cu:ZnS film showed an average transparency of 70% in visible range but low hole conductivity. Very recently, Ortíz-Ramos et al.[36] reported chemical bath deposition of Cu doped ZnS films. At a reported composition of $Cu_{0.1}Zn_{0.9}S$ the optical transparency was ca. 70% but the sheet resistance was relatively high, 1.73×10^5 Ω/□. Although optical transparency has been achieved for p-type CuZnS films, their low conductivity currently limits application in electronic devices.

In this work, we synthesized the full composition range (x = 1 to x = 0) of the $(CuS)_x$:$(ZnS)_{1-x}$ nanocomposite system via chemical bath deposition with the aim of maximizing both transparency and hole conductivity. By selection of the proper complexing agent, codeposition of ZnS and CuS was achieved. By adjusting the concentration of the complexing agent, the crystallite size of the films can be tuned in order to optimize the transparency. We also show that the hole conductivity is linked to the proportion of the CuS phase. In this way, p-type transparent, highly conductive (maximum >1000 S/cm, sheet resistance ~200 Ω/□) films of nanocrystalline CuS–ZnS composites were achieved. Notably, the hole conductivity is much higher than that of the state-of-the-art p-type TCMs.

As a potential application of a highly conducting p-TCM, we investigated their use in solar cells. In recent years, considerable effort has been devoted to developing hole-selective contacts to Si as an alternative to traditional homojunctions formed by doping, as exemplified by the amorphous Si/Si heterojunction in the "heterojunction with intrinsic layer thin-layer" (HIT) approach originally developed by Sanyo.[37,38] Simpler approaches have been investigated as well. Hybrid c-Si/organic structures, such as PEDOT:PSS, haver been demonstrated to achieve open circuit voltages (V_{oc}) of up to 570 mV.[39] However, they often suffer from environmental instability. Transition oxides, such as MO_x[40] and WO_3,[41] were recently reported to function as hole-selective contacts to n-Si with an impressive V_{oc} of ~580 mV. However, their fabrication process typically requires vacuum processing. Carbon nanotubes and graphene have also been employed and open circuit voltages up to 550 mV have been observed.[42−51] Here, we investigated chemical-bath-deposited-$(CuS)_x$:$(ZnS)_{1-x}$ as a hole-selective contact to n-Si. Several proof-of-concept photovoltaic (PV) devices based on p-$(CuS)_x$:$(ZnS)_{1-x}$/n-Si were fabricated, and observed optimal 1 sun V_{oc} value of 535 mV and J_{sc} value 21 mA/cm^2, which suggests the potential for this material in photovoltaic devices and other optoelectronic devices.

Synthesis Strategy. Several competitive processes that are related to synthesis conditions (e.g., precursor concentration, complexing agent, and stirring rate) occur at the same time in chemical bath deposition, as shown schematically in Figure 1.[32,52] In particular, both homogeneous nucleation, which leads

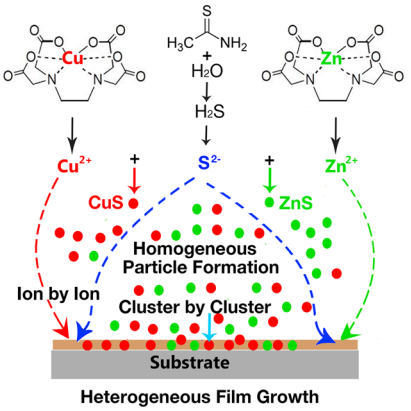

Figure 1. Schematic illustration of the growth mechanism of $(CuS)_x$:$(ZnS)_{1-x}$ films via chemical bath deposition. Homogeneous nucleation of CuS and ZnS nanoparticles is represented by red and green dots, respectively. This process leads to cluster by cluster film growth (cyan arrow). The ion by ion growth process is represented by the dashed red and green arrows.

to particle formation in solution, and heterogeneous nucleation, which results in film formation on the substrate, can occur simultaneously. Moreover, film growth can occur via an ion-by-ion process or by deposition of clusters formed as a result of homogeneous nucleation. To obtain smooth and continuous films, it is desirable to have heterogeneous nucleation followed by ion-by-ion growth. Thus, the suppression of cluster-by-cluster growth is essential for the formation of good-quality films in CBD.[53] In principle, ion-by-ion growth becomes dominant when the activity of the reacting cations and anions is higher than that of the particles in solution.[54]

The CBD growth mechanism of metal sulfide (MS) thin films is well-known as the product of the reaction between M-[complexing agent]$^{x+}$ ions and S^{2-} ions in solution or on the substrate surface.[55,56] Because the K_{sp} (solubility product at room temperature) of CuS (5×10^{-48}) is much lower than that of ZnS (3×10^{-24}),[57] CuS would be expected to have a much larger deposition rate. Thus, the complexing agent plays a critical role not only in the growth rate of the films but also in

DOI: 10.1021/acs.nanolett.5b05124
Nano Lett. 2016, 16, 1925−1932

influencing the stoichiometry and crystal size because it controls the release rate of metal ion in the reaction process.[58] Here, we used Na_2EDTA, a nontoxic and inexpensive complexing agent. It has been used to make high-quality nanocrystalline metal sulfide films.[59,60] Compared with other complexing agents, such as Na_3-citrate, which has a relatively stronger binding to Zn^{2+},[55] ETDA forms a stronger complex with Cu^{2+} (stability constant = 18.8) compared to the complex with Zn^{2+} (16.5), so it will function to slow down the precipitation of CuS, allowing codeposition of CuS and ZnS despite their difference in K_{sp} values.

Structural and Morphology Analysis. $(CuS)_x:(ZnS)_{1-x}$ films were synthesized by chemical bath deposition at a low temperature (80 °C) for 1 h (See Supporting Information for detailed description of growth conditions and measurement of the growth rate). A series of films of the similar thickness (~50 nm) with various Cu concentrations, from $x = 0$ to $x = 1$ (x is the molar ratio of Cu to (Cu + Zn)), were obtained by changing the starting ratio of Cu precursor to Zn precursor. Particle induced X-ray emission (PIXE) was used to determine the stoichiometry of films, whereas Rutherford backscattering spectrometry (RBS) was utilized to measure the thickness of the films.

Figure 2 shows plan-view transmission electron micrographs (TEM) of the $(CuS)_x:(ZnS)_{1-x}$ films with x varying from 0 to

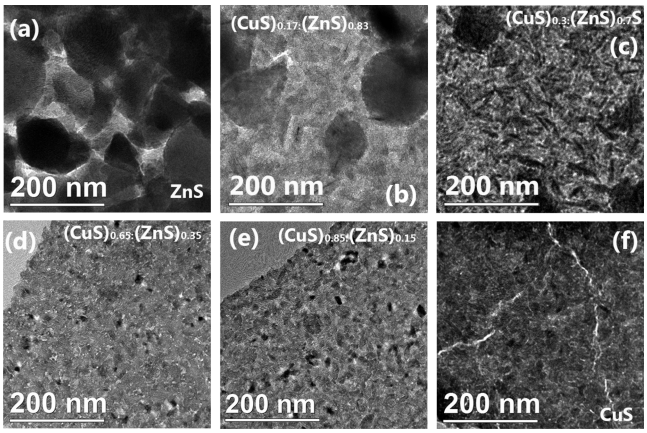

Figure 2. TEM images of nanocomposite $(CuS)_x:(ZnS)_{1-x}$ film with different Cu concentrations: (a) $x = 0$; (b) $x = 0.17$; (c) $x = 0.3$; (d) $x = 0.65$; (e) $x = 0.85$; (f) $x = 1$.

1. It can be seen clearly that the Cu concentration plays an important role in the microstructure of the films. Pure ZnS films ($x = 0$) of compact large nanoparticles are formed with sizes ranging from 100 to 150 nm. As the Cu content is increased to 30%, Figure 2b,c, the films are mainly assemblies of tightly bound tiny grains with several protruding larger aggregates scattered within the films. It is also seen, with increased Cu concentration, that the shape of the small grains forming the matrix becomes elongated, whereas the size of the dispersed aggregates becomes smaller. With further increases in the Cu content, as can be seen from Figure 2d,e,f, the films composed of smaller granules (<10 nm) are more uniform and smooth, with no observation of larger aggregates as that of Zn rich samples. The $(CuS)_{0.65}:(ZnS)_{0.35}$ film shown in Figure 2d shows the best uniformity with the smallest grain sizes, which can also be seen from the corresponding AFM images in Figure S2 and SEM images in Figure S3.

Wide-angle X-ray scattering (WAXS) was used to identify the crystalline phases present in the films. Shown in Figure 3,

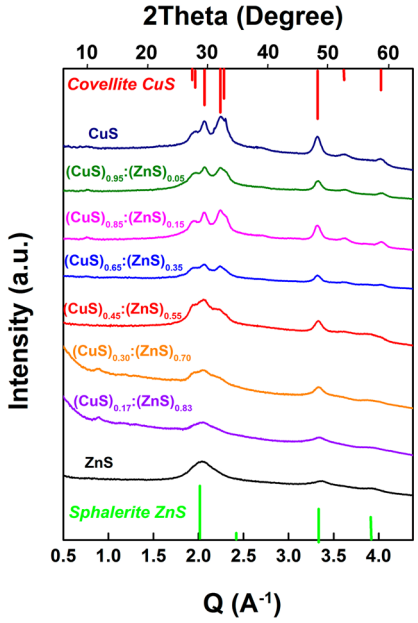

Figure 3. WAXS patterns of $(CuS)_x:(ZnS)_{1-x}$ film at different Cu concentrations, from $x = 0$ to $x = 1$. The expected peak positions of covellite CuS and sphalerite ZnS are indicated by lines at the top and bottom of the plot, respectively.

sphalerite ZnS is detected in ZnS reference sample. In the Cu concentration range $0 < x < 0.45$, the signature peaks of sphalerite ZnS are gradually weakened, whereas the mixed phases of sphalerite ZnS and covellite CuS can be seen for sample $(CuS)_{0.45}:(ZnS)_{0.55}$. When further increasing x, covellite CuS becomes dominant and no obvious ZnS phase can be seen. This phase evolution is also consistent with the result obtained from selected area electron diffractions (SAED), as shown in Figure S5. It is also interesting to notice the broadening trend of the peaks before x reaches 0.65, indicating diminishing crystallite size. The average correlation length of these samples is less than 10 nm. Afterward, the peaks become slightly narrowed due to the larger nanocrystals, which agrees well with the results of the TEM images. The calculated average nanocrystal size for each film can be seen in Figure S6. Some degree of oxidation is seen in these films from observing the sulfur K-edge in XANES as shown in Figure S11. It may result from dissolved oxygen in the growth solution.

Optical Properties. Figure 4 shows the optical transmittance and estimated band gap of $(CuS)_x:(ZnS)_{1-x}$ nanocomposite films. Pure ZnS film has a band gap of 3.6 eV, close to literature reports.[61,62] Also, as expected, CuS films have an optical gap of ~2.1 eV and <40% transmission in the visible region. The direct band gap of CuS (2.1 eV) matches well with previously reported values.[63] All of the nanocomposite films have higher transparency than that of CuS. For example, the $(CuS)_{0.65}:(ZnS)_{0.35}$ has a peak transparency near 600 nm of 75% and is nearly as transparent as the ZnS control film. In Zn rich samples, from $0 < x < 0.3$, the transmittance decreases with increasing Cu content. For $(CuS)_x:(ZnS)_{1-x}$ films ($0.3 < x < 1$), the transparency becomes dependent on the crystal domain size of the films. Smaller crystallites were found for $x > 0.5$, with larger crystallites at lower CuS content.

DOI: 10.1021/acs.nanolett.5b05124
Nano Lett. 2016, 16, 1925−1932

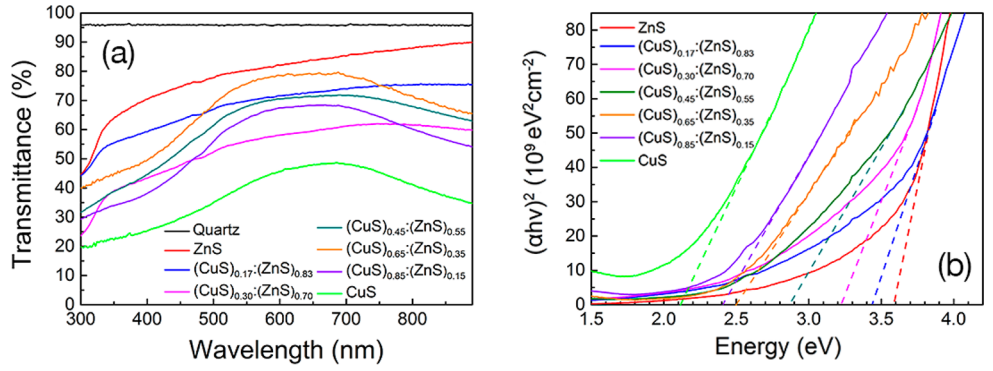

Figure 4. (a) Transmission spectra of $(CuS)_x:(ZnS)_{1-x}$ film (thickness ~50 nm) and (b) Tauc plot of $(CuS)_x:(ZnS)_{1-x}$ at different Cu concentrations, from $x = 0$ to $x = 1$.

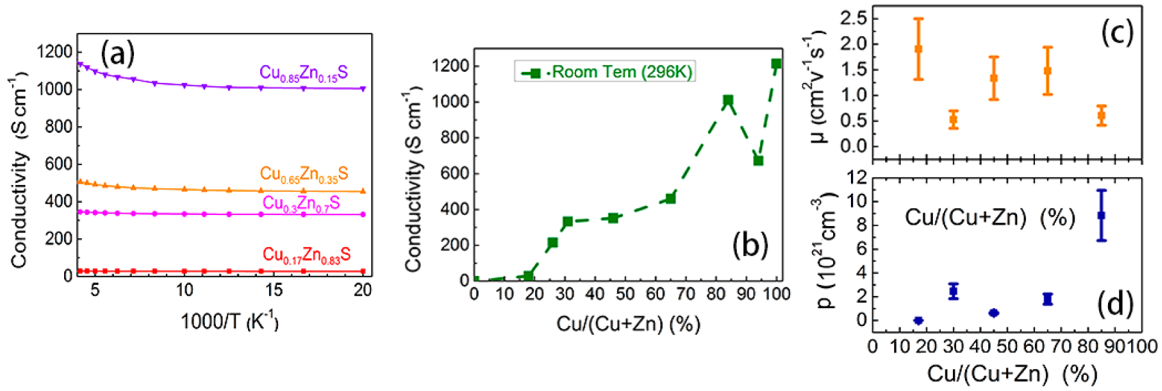

Figure 5. (a) Hole conductivity of the $(CuS)_x:(ZnS)_{1-x}$ films at different Cu concentrations as a function of temperature; (b) Hole conductivity, (c) Carrier mobility and (d) Carrier concentrations of the $(CuS)_x:(ZnS)_{1-x}$ nanocomposite films at room temperature as a function of Cu concentrations from AC Hall measurements.

As shown in Figure 4a, the film transmittance does not increase monotonically with ZnS content, which suggests that more than one factor play a role in transparency. In CuS films, it has been reported that smaller crystallites lead to higher transparency by minimizing scattering losses.[64] Here, as the crystal sizes of some films are just a few nanometers, such as $(CuS)_{0.65}:(ZnS)_{0.35}$ has an average nanocomposite size of <5 nm (see HRTEM Image in Supporting Information Figure S5 and Scherrer calculation in Figure S6), the quantum confinement effect should be also considered as it can further improve the transparency as a result of lower absorption. Control experiments were conducted to investigate this hypothesis. At nearly the same x (0.85 ± 0.02) in $(CuS)_x:(ZnS)_{1-x}$, we controlled the crystallite size through the adjustment of complexing agent concentration and observed that the transmission varied between 45% for the largest crystallites and 65% for the smallest (Figures S7 and S8). This experimental result correlates well with first-principles calculations of the exciton energies as a function of quantum dot size, which predict increases in the band gap and optical transmission for diameters less than 5 nm.[65]

To estimate the direct optical gap, Tauc plots generated from the absorption coefficients are utilized, as shown in Figure 4b. Starting from CuS, the band gap is opened by introduction of ZnS into the system, with the range of 2.1 to 3.6 eV achievable by controlling the Cu concentration. It is noteworthy that the optical band gap of many of the $(CuS)_x:(ZnS)_{1-x}$ films is larger than previously reported for $Cu_{0.6}Zn_{0.4}S$ (2.14 eV)[66] films due to the quantum size effect caused by the much smaller grains produced here.

Electrical Properties. As indicated by Hall and Seebeck coefficient measurements (see Figure S9), all the $(CuS)_x:(ZnS)_{1-x}$ films, except for $x = 0$, display p-type conductivity. For each composition, more than three samples were prepared and tested to ensure the reproducibility of the conductivity. Overall, the hole conductivity is found to be positively correlated to Cu concentration as can be seen in Figure 5b. A maximum conductivity of more than 1000 S/cm in films with $x = 0.85$ was measured, which is much higher than most of the reported p-TCMs.[17,27] It is interesting that the conductivity of the film with $x = 0.95$ is lower than that of both the $x = 0.85$ film and a pure CuS_x film; we do not know the origin of this effect. Hole concentration p and mobility μ were measured with a recently developed rotating parallel dipole line (PDL) Hall system.[67] It operates based on lock-in detection of the Hall signal under an oscillating magnetic field. The sensitivity of this system is key to extracting the small Hall signals of low mobility films like our $(CuS)_x:(ZnS)_{1-x}$ layers. As shown in Figure 5c, μ appears to increase gradually with Cu concentration, within the range of $0.17 < x < 0.65$, and then decrease. Compared with other samples, the high conductivity of the most transparent film $(CuS)_{0.65}:(ZnS)_{0.35}$ comes from the relatively higher mobility. In Figure 5d, p varies from $(1-10) \times 10^{21}$ cm^3, which is in the range of a degenerately doped semiconductor. As shown Figure 5a, the conductivity is independent of temperature which confirms the degenerate hole conductivity. This type of band conduction is similar to some other p-type

DOI: 10.1021/acs.nanolett.5b05124
Nano Lett. 2016, 16, 1925−1932

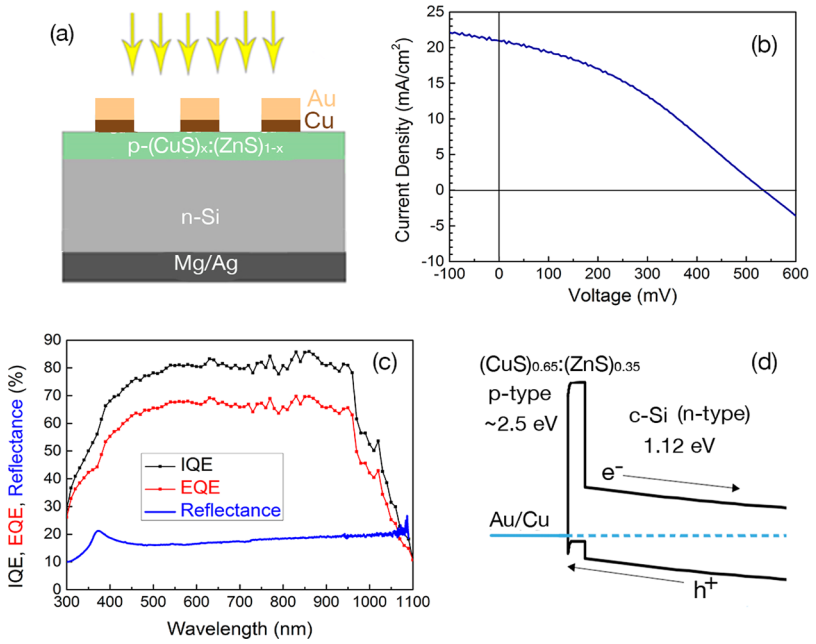

Figure 6. (a) Schematic illustration of the structure of $(CuS)_{0.65}$:$(ZnS)_{0.35}$ thin film solar cell. (b) The $J-V$ characteristics of $(CuS)_{0.65}$:$(ZnS)_{0.35}$ thin film solar cell device fabricated via chemical bath deposition. (c) EQE, IQE, and reflectance of the $(CuS)_{0.65}$:$(ZnS)_{0.35}$ thin film solar cell. (d) Schematic energy band diagrams of the heterojunction of $(CuS)_{0.65}$:$(ZnS)_{0.35}$ and n-type silicon.

metallic conductors, such as $CuAlS_2$.[19] Furthermore, the valence band maximum (VBM) which aligns with the Fermi level, as deduced from the XPS measurements shown in Figure S10, again suggests the degenerate conductivity of $(CuS)_x$:$(ZnS)_{1-x}$ films.

Figure 5 reveals that although the mobility of 0.5−2.0 cm^2 V^{-1} s^{-1} is comparable to previously studied p-type transparent materials such as $CuAlO_2$,[68] Li:Cr_2MnO_4,[69] and Mg:Cr_2O_3,[27] the hole concentration is substantially higher ($1-9 \times 10^{21}$ cm^{-3}) and is responsible for the overall higher hole conductivity. Covellite CuS is well known as a p-type conductor.[70,71] Despite the simplicity of its chemical formula, CuS has a complex structure consisting of alternating planar CuS layers and Cu_2S_2 double layers.[71] In this copper-deficient compound, it is the copper vacancies that leads to the high hole concentration.[72,73] Thus, we attribute the hole conduction in $(CuS)_x$:$(ZnS)_{1-x}$ nanocomposite films to the CuS phase. The conducting network formed by CuS (even in Zn rich samples) produces the degenerate p-type conductivity in the films.

As discussed above, transparency is dependent on both Cu content and crystal sizes, whereas Cu content plays an important role in the hole conductivity as well. The trade-off between conductivity and transparency is illustrated in Figure S12. Of the films with <1000 Ω/□ sheet resistance, the highest transmission is found at $x = 0.65$ (smallest crystallite size, Figure S6) and the lowest sheet resistance is found at $x = 0.85$. To maximize the properties of p-type TCM, it is seen to be beneficial to increase the Cu concentration to achieve high p-type conductivity while maintaining the transparency by decreasing the grain sizes within the films. This is the key to high hole conductivity with relatively good transparency in p-type TCMs.

Photovoltaic Devices. To demonstrate the application of p-$(CuS)_x$:$(ZnS)_{1-x}$ films in PV devices, several proof-of concept $(CuS)_x$:$(ZnS)_{1-x}$/Si heterojunction solar cells were fabricated. The schematic structure of a typical heterojunction is shown in Figure 6a. Further fabrication details and a description of the optimization process are contained in the Supporting Information. Notably, we found that a ∼100 nm $(CuS)_x$:$(ZnS)_{1-x}$ film made with two consecutive CBD steps provided superior performance. Ohmic grid contacts on p-$(CuS)_x$:$(ZnS)_{1-x}$ were achieved by electron-beam evaporating Cu/Au (4 nm/60 nm) as front contacts, whereas Mg/Ag composite (100 nm) was thermally evaporated as the back contact to n-Si. The $J-V$ behavior, which was measured under standard test conditions (1000 W/m^2, air mass 1.5 global ($AM1.5_g$) spectrum and 25 °C) for the 1 × 1 cm^2 device, is shown in Figure 6a. For the p-$(CuS)_{0.65}$:$(ZnS)_{0.35}$/n-Si device, a J_{SC} and V_{OC} of 21 mA/cm^2 and 535 mV were observed. The obvious effects of both series and shunt resistances are seen resulting in a modest fill factor (FF). The shunt path is likely to arise from pinholes in the solution-prepared thin film, which can potentially be improved by optimization. The series resistance from both the front and back contacts is the main factor that inhibits the performance of the device.

The external quantum efficiency (EQE) and internal quantum efficiency (IQE) are shown in Figure 6c. The IQE is 80% or higher throughout most of the visible range, indicating efficient collection of holes via the heterointerface, particularly for those generated near the surface (short wavelength). The EQE is similar to that reported for graphene/n-Si junctions.[50] The rectifying behavior in the dark and photocurrent under one sun of the p-$(CuS)_{0.65}$:$(ZnS)_{0.35}$/n-Si device can be understood via the schematic energy band structure of this heterostructure depicted in Figure 6d. An asymmetrical energy barrier, which is formed at the interface of the heterojunction due to the differences in the band gap structures, electron affinity and work function of $Cu_{0.65}Zn_{0.35}S$ and Si, allows the low resistance collection of holes and simultaneous blocking of electrons.[74]

Although our simple heterojuncton Si PV device with a nonpassivated interface cannot be expected to rival the performance of the state-of-art commercial heterojunction silicon solar cells, which typically employ a sophisticated silicon

DOI: 10.1021/acs.nanolett.5b05124
Nano Lett. 2016, 16, 1925−1932

passivation structure,[38] it clearly shows the potential of the transparent, conductive $(CuS)_x$:$(ZnS)_{1-x}$ film as a hole contact to n-type silicion. With a demonstrated V_{OC} of 535 mV, the V_{OC} of our p-$(CuS)_x$:$(ZnS)_{1-x}$/n-Si device is comparable to that of the best-in-class single-walled carbon nanotube/Si (530 mV)[75] (where the reported V_{OC} of SWCN/Si devices is within the range of 370−530 mV)[42−44,46] and graphene/Si (540 mV)[50] PV devices (where the reported V_{OC} of graphene/Si device is within the range of 359−540 mV).[47−49]

Given the fact that antireflection or light trapping was not considered in this cell, as can be seen from the reflectance spectrum in Figure 6c, various promising improvements can be envisioned. For example, as the performance of the cells is mainly limited by fill factor—which results from the non-optimized film thickness—front and back contact, and band alignment of $(CuS)_x$:$(ZnS)_{1-x}$ and silicon. The thickness and composition of $(CuS)_x$:$(ZnS)_{1-x}$ film can be tuned to improve the performance. A passivation layer with $(CuS)_x$:$(ZnS)_{1-x}$ contact openings or patterned back grid in combination with a passivating dielectric can be implemented in the cell structure to improve the V_{OC}. A higher J_{sc} can be acquired by taking light-trapping structures or the antireflection layer into consideration.

In summary, we have fabricated p-type transparent, highly conductive p-$(CuS)_x$:$(ZnS)_{1-x}$ nanocomposite films via the simple, low-cost chemical bath deposition. We achieved a very high hole conductivity >1000 S/cm with x = 0.85, similar to PVD-deposited FTO[76] and AZO[77,78] at a similar process temperature. An optical transparency of around 67% is obtained for film thickness of 50 nm. We find the key to hole conductivity in this system is the covellite CuS phase, which forms the network of hole carriers. At the same composition, the key to transparency is to minimize the crystal sizes of the films, as smaller crystal domains will not only reduce light scattering but also widen the band gap of the films due to the quantum effect. These films were also demonstrated on simple PV devices. An optimal V_{OC} value of 535 mV and J_{sc} values of 21 mA/cm^2 were achieved with a p-$(CuS)_x$:$(ZnS)_{1-x}$/n-Si device.

The development of p-type transparent conducting $(CuS)_x$:$(ZnS)_{1-x}$ film and demonstration of simple silion heterojunction PV devices meet the desire of the industry for a low-cost, low-temperature, fully solution-processed cell architecture. The combination of high p-type conductivity, high transparency, and a low-cost, low-temperature synthesis method for $(CuS)_x$:$(ZnS)_{1-x}$ may also widely open the design space for new device applications, such as flexible electronics, hole transport layers in halide perovskite solar cells, recombination layers in tandem solar cells, and self-powered UV detectors.

■ ASSOCIATED CONTENT

Supporting Information

The Supporting Information is available free of charge on the ACS Publications website at DOI: 10.1021/acs.nanolett.5b05124.

Synthesis procedure; characterization details; growth rate; atomic force microscopy; SEM plan view and cross-section image; TEM, HRTEM, and SAED; Scherrer calculation of average crystal size; effect of Na_2ETDA on morphology and transparency; Seebeck coefficient measurements; XPS measurement; S edge XANES spectra; transparency and conductivity of nanocomposite films as a function of composition; additional PV devices. (PDF)

■ AUTHOR INFORMATION

Corresponding Author

*E-mail: JWAger@lbl.gov.

Author Contributions

The manuscript was written through contributions of all authors. All authors have given approval to the final version of the manuscript.

Notes

The authors declare no competing financial interest.

■ ACKNOWLEDGMENTS

The authors appreciated helpful discussions and technical support from Kunrong Xu, Aizhao Pan, and Rachel Woods-Robinson. Chemical bath deposition and electronic characterization were performed in the Electronic Materials Program, which is supported by the Director, Office of Science, Office of Basic Energy Sciences, Materials Sciences and Engineering Division, of the U.S. Department of Energy under Contract No. DE-AC02-05CH11231, which is supported by Division of Materials Science, Office of Science, DOE. Solar cell fabrication and characterization were supported by the Department of Energy through the Bay Area Photovoltaic Consortium under Award Number DE-EE0004946. X-ray photoelectron spectroscopy was performed in collaboration with the Joint Center for Artificial Photosynthesis (JCAP), a DOE Energy Innovation Hub, supported through the Office of Science of the U.S. Department of Energy under Award Number DE-SC0004993. AC Hall effect measurements were performed at Nanyang Technological University with support from the Singapore Berkeley Initiative for Sustainable Energy (SinBeRISE). Use of the Stanford Synchrotron Radiation Lightsource, SLAC National Accelerator Laboratory, is supported by the U.S. Department of Energy, Office of Science, Office of Basic Energy Sciences under Contract No. DE-AC02-76SF00515. X.J.X. acknowledges fellowship support from the Chinese Scholarship Council.

■ REFERENCES

(1) Beyer, W.; Hüpkes, J.; Stiebig, H. *Thin Solid Films* **2007**, *516*, 147−154.
(2) Rowell, M. W.; McGehee, M. D. *Energy Environ. Sci.* **2011**, *4*, 131−134.
(3) Liu, H.; Avrutin, V.; Izyumskaya, N.; Özgur, Ü.; Morkoç, H. *Superlattices Microstruct.* **2010**, *48*, 458−484.
(4) Fortunato, E.; Barquinha, P.; Martins, R. *Adv. Mater.* **2012**, *24*, 2945−2986.
(5) Ellmer, K. *Nat. Photonics* **2012**, *6*, 809−817.
(6) Nomura, K.; Ohta, H.; Takagi, A.; Kamiya, T.; Hirano, M.; Hosono, H. *Nature* **2004**, *432*, 488−492.
(7) Lin, H.; Li, L.; Ren, J.; Cai, Z.; Qiu, L.; Yang, Z.; Peng, H. *Sci. Rep.* **2013**, *3*, 1−6.
(8) Mryasov, O.; Freeman, A. *Phys. Rev. B: Condens. Matter Mater. Phys.* **2001**, *64*, 2−4.
(9) Yeon Kwon, J.; Kyeong Jeong, J. *Semicond. Sci. Technol.* **2015**, *30*, 024002.
(10) Alves, A. C. T.; Gomes, D. J. C.; Silva, J. R.; Silva, G. B. *Appl. Surf. Sci.* **2013**, *279*, 67−70.
(11) Kent, C. A.; Concepcion, J. J.; Dares, C. J.; Torelli, D. A.; Rieth, A. J.; Miller, A. S.; Hoertz, P. G.; Meyer, T. J. *J. Am. Chem. Soc.* **2013**, *135*, 8432−8435.

DOI: 10.1021/acs.nanolett.5b05124
Nano Lett. 2016, 16, 1925−1932

(12) Lee, S. H.; Han, S. H.; Jung, H. S.; Shin, H.; Lee, J.; Noh, J. H.; Lee, S.; Cho, I. S.; Lee, J. K.; Kim, J.; Shin, H. *J. Phys. Chem. C* **2010**, *114*, 7185−7189.
(13) Grilli, M. L.; Sytchkova, A.; Boycheva, S.; Piegari, A. *Phys. Status Solidi A* **2013**, *210*, 748−754.
(14) Hautier, G.; Miglio, A.; Ceder, G.; Rignanese, G.-M.; Gonze, X. *Nat. Commun.* **2013**, *4*, 2292.
(15) Delahoy, A. E.; Guo, S. In *Handbook of Photovoltaic Science and Engineering*; Luque, A., Hegedus, S., Eds.; John Wiley & Sons, Ltd.: Weinheim, Germany, 2011; pp 716−796.
(16) Kawazoe, H.; Yasukawa, M.; Hyodo, H.; Kurita, M.; Yanagi, H.; Hosono, H. *Nature* **1997**, *389*, 939−942.
(17) Banerjee, A. N.; Chattopadhyay, K. K. *Prog. Cryst. Growth Charact. Mater.* **2005**, *50*, 52−105.
(18) Kawazoe, H.; Yanagi, H.; Ueda, K.; Hosono, H. *MRS Bull.* **2000**, *25*, 28−36.
(19) Sheng, S.; Fang, G.; Li, C.; Xu, S.; Zhao, X. *Phys. Status Solidi A* **2006**, *203*, 1891−1900.
(20) Nagarajan, R.; Draeseke, A. D.; Sleight, A. W.; Tate, J. *J. Appl. Phys.* **2001**, *89*, 8022.
(21) Ruttanapun, C.; Prachamon, W.; Wichainchai, A. *Curr. Appl. Phys.* **2012**, *12*, 166−170.
(22) Hiramatsu, H.; Ueda, K.; Ohta, H.; Orita, M.; Hirano, M.; Hosono, H. *Thin Solid Films* **2002**, *411*, 125−128.
(23) Chen, L.; Yang, J.; Klaus, S.; Lee, L. J.; Woods-Robinson, R.; Ma, J.; Lum, Y.; Cooper, J. K.; Toma, F. M.; Wang, L.-W.; Sharp, I. D.; Bell, A. T.; Ager, J. W. *J. Am. Chem. Soc.* **2015**, *137*, 9595−9603.
(24) Asbalter, J.; Subrahmanyam, A. *J. Vac. Sci. Technol., A* **2000**, *18*, 1672.
(25) Kudo, A.; Yanagi, H.; Hosono, H.; Kawazoe, H. *Appl. Phys. Lett.* **1998**, *73*, 220.
(26) Caraveo-Frescas, J. A.; Nayak, P. K.; Al-Jawhari, H. A.; Granato, D. B.; Schwingenschlögl, U.; Alshareef, H. N. *ACS Nano* **2013**, *7*, 5160−5167.
(27) Farrell, L.; Fleischer, K.; Caffrey, D.; Mullarkey, D.; Norton, E.; Shvets, I. V. *Phys. Rev. B: Condens. Matter Mater. Phys.* **2015**, *91*, 125202.
(28) Han, J.; Spanheimer, C.; Haindl, G.; Fu, G.; Krishnakumar, V.; Schaffner, J.; Fan, C.; Zhao, K.; Klein, A.; Jaegermann, W. *Sol. Energy Mater. Sol. Cells* **2011**, *95*, 816−820.
(29) Panthani, M. G.; Kurley, J. M.; Crisp, R. W.; Dietz, T. C.; Ezzyat, T.; Luther, J. M.; Talapin, D. V. *Nano Lett.* **2014**, *14*, 670−675.
(30) Aegerter, M. A.; Almeida, R.; Soutar, A.; Tadanaga, K.; Yang, H.; Watanabe, T. *J. Sol-Gel Sci. Technol.* **2008**, *47*, 203.
(31) Tsui, K.-H.; Lin, Q.; Chou, H.; Zhang, Q.; Fu, H.; Qi, P.; Fan, Z. *Adv. Mater.* **2014**, *26*, 2805−2811.
(32) Mane, R. S.; Lokhande, C. D. *Mater. Chem. Phys.* **2000**, *65*, 1−31.
(33) Kudo, A.; Sekizawa, M. *Catal. Lett.* **1999**, *58*, 241−243.
(34) Diamond, A. M.; Corbellini, L.; Balasubramaniam, K. R.; Chen, S.; Wang, S.; Matthews, T. S.; Wang, L.-W.; Ramesh, R.; Ager, J. W. *Phys. Status Solidi A* **2012**, *209*, 2101−2107.
(35) Yang, K.; Nakashima, Y.; Ichimura, M. *J. Electrochem. Soc.* **2012**, *159*, H250.
(36) Ortíz-Ramos, D. E.; González, L. A.; Ramirez-Bon, R. *Mater. Lett.* **2014**, *124*, 267−270.
(37) De Wolf, S.; Descoeudres, A.; Holman, Z. C.; Ballif, C. *Green* **2012**, *2*, 7−24.
(38) Taguchi, M.; Yano, A.; Tohoda, S.; Matsuyama, K.; Nakamura, Y.; Nishiwaki, T.; Fujita, K.; Maruyama, E. *IEEE J. Photovoltaics* **2014**, *4*, 96−99.
(39) Nagamatsu, K. A.; Avasthi, S.; Jhaveri, J.; Sturm, J. C. *IEEE J. Photovoltaics* **2014**, *4*, 260−264.
(40) Battaglia, C.; Yin, X.; Zheng, M.; Sharp, I. D.; Chen, T.; McDonnell, S.; Azcatl, A.; Carraro, C.; Ma, B.; Maboudian, R.; Wallace, R. M.; Javey, A. *Nano Lett.* **2014**, *14*, 967−971.
(41) Bivour, M.; Temmler, J.; Steinkemper, H.; Hermle, M. *Sol. Energy Mater. Sol. Cells* **2015**, *142*, 34−41.
(42) Ong, P.-L.; Euler, W. B.; Levitsky, I. A. *Nanotechnology* **2010**, *21*, 105203.
(43) Jia, Y.; Cao, A.; Bai, X.; Li, Z.; Zhang, L.; Guo, N.; Wei, J.; Wang, K.; Zhu, H.; Wu, D.; Ajayan, P. M. *Nano Lett.* **2011**, *11*, 1901−1905.
(44) Tune, D. D.; Flavel, B. S.; Krupke, R.; Shapter, J. G. *Adv. Energy Mater.* **2012**, *2*, 1043−1055.
(45) Jung, Y.; Li, X.; Rajan, N. K.; Taylor, A. D.; Reed, M. A. *Nano Lett.* **2013**, *13*, 95−99.
(46) Chen, L.; Yu, H.; Zhong, J.; He, H.; Zhang, T. *Electrochim. Acta* **2015**, *178*, 732−738.
(47) Li, X.; Zhu, H.; Wang, K.; Cao, A.; Wei, J.; Li, C.; Jia, Y.; Li, Z.; Li, X.; Wu, D. *Adv. Mater.* **2010**, *22*, 2743−2748.
(48) Feng, T.; Xie, D.; Lin, Y.; Zang, Y.; Ren, T.; Song, R.; Zhao, H.; Tian, H.; Li, X.; Zhu, H.; Liu, L. *Appl. Phys. Lett.* **2011**, *99*, 233505.
(49) Fan, G.; Zhu, H.; Wang, K.; Wei, J.; Li, X.; Shu, Q.; Guo, N.; Wu, D. *ACS Appl. Mater. Interfaces* **2011**, *3*, 721−725.
(50) Miao, X.; Tongay, S.; Petterson, M. K.; Berke, K.; Rinzler, A. G.; Appleton, B. R.; Hebard, A. F. *Nano Lett.* **2012**, *12*, 2745−2750.
(51) Cui, T.; Lv, R.; Huang, Z.-H.; Chen, S.; Zhang, Z.; Gan, X.; Jia, Y.; Li, X.; Wang, K.; Wu, D.; Kang, F. *J. Mater. Chem. A* **2013**, *1*, 5736.
(52) Jayasree, Y.; Chalapathi, U.; Uday Bhaskar, P.; Raja, V. S. *Appl. Surf. Sci.* **2012**, *258*, 2732−2740.
(53) *Chemical Solution Deposition of Functional Oxide Thin Films*; Schneller, T., Waser, R., Eds.; Springer: New York, 2013; pp 233−261.
(54) Zhang, H.; Ma, X.; Yang, D. *Mater. Lett.* **2004**, *58*, 5−9.
(55) Shin, S. W.; Agawane, G. L.; Gang, M. G.; Moholkar, A. V.; Moon, J. H.; Kim, J. H.; Lee, J. Y. *J. Alloys Compd.* **2012**, *526*, 25−30.
(56) O'Brien, P.; McAleese, J. *J. Mater. Chem.* **1998**, *8*, 2309−2314.
(57) Gharabaghi, M.; Irannajad, M.; Azadmehr, A. R. *Ind. Eng. Chem. Res.* **2012**, *51*, 954−963.
(58) Prem kumar, T.; Sankaranarayanan, K. *Can. J. Chem. Eng.* **2013**, *91*, 27−33.
(59) Ubale, A. U.; Sakhare, Y. S.; Bombatkar, S. M. *Mater. Res. Bull.* **2013**, *48*, 3564−3571.
(60) Goudarzi, A.; Aval, G. M.; Sahraei, R.; Ahmadpoor, H. *Thin Solid Films* **2008**, *516*, 4953−4957.
(61) Fang, X.; Zhai, T.; Gautam, U. K.; Li, L.; Wu, L.; Bando, Y.; Golberg, D. *Prog. Mater. Sci.* **2011**, *56*, 175−287.
(62) Xu, X.; Hu, L.; Gao, N.; Liu, S.; Wageh, S.; Al-Ghamdi, A. A.; Alshahrie, A.; Fang, X. *Adv. Funct. Mater.* **2015**, *25*, 445−454.
(63) Zhang, J.; Yu, J.; Zhang, Y.; Li, Q.; Gong, J. R. *Nano Lett.* **2011**, *11*, 4774−4779.
(64) Lu, Y.; Meng, X.; Yi, G.; Jia, J. *J. Colloid Interface Sci.* **2011**, *356*, 726−733.
(65) Li, J. B.; Wang, L.-W. W. *Phys. Rev. B: Condens. Matter Mater. Phys.* **2005**, *72*, 125325.
(66) Ali Yildirim, M.; Ateş, A.; Astam, A. *Phys. E* **2009**, *41*, 1365−1372.
(67) Gunawan, O.; Virgus, Y.; Tai, K. F. *Appl. Phys. Lett.* **2015**, *106*, 062407.
(68) Yu, R.-S.; Yin, H.-H. *Thin Solid Films* **2012**, *526*, 103−108.
(69) Peng, H.; Zakutayev, A.; Lany, S.; Paudel, T. R.; D'Avezac, M.; Ndione, P. F.; Perkins, J. D.; Ginley, D. S.; Nagaraja, A. R.; Perry, N. H.; Mason, T. O.; Zunger, A. *Adv. Funct. Mater.* **2013**, *23*, 5267−5276.
(70) Liang, W.; Whangbo, M.-H. *Solid State Commun.* **1993**, *85*, 405−408.
(71) Conejeros, S.; Moreira, I. D. P. R.; Alemany, P.; Canadell, E. *Inorg. Chem.* **2014**, *53*, 12402−12406.
(72) Yuan, K. D.; Wu, J. J.; Liu, M. L.; Zhang, L. L.; Xu, F. F.; Chen, L. D.; Huang, F. Q. *Appl. Phys. Lett.* **2008**, *93*, 132106.
(73) Morales-García, A.; Soares, A. L.; Dos Santos, E. C.; de Abreu, H. A.; Duarte, H. A. *J. Phys. Chem. A* **2014**, *118*, 5823−5831.
(74) Tang, Y. B.; Chen, Z. H.; Song, H. S.; Lee, C. S.; Cong, H. T.; Cheng, H. M.; Zhang, W. J.; Bello, I.; Lee, S. T. *Nano Lett.* **2008**, *8*, 4191−4195.
(75) Jung, Y.; Li, X.; Rajan, N. K.; Taylor, A. D. A.; Reed, M. A. *Nano Lett.* **2013**, *13*, 95−99.

DOI: 10.1021/acs.nanolett.5b05124
Nano Lett. 2016, 16, 1925−1932

(76) Liao, B.-H.; Chan, S.-H.; Lee, C.-C.; Chen, S.-H.; Chiang, D. *Opt. Interface Coatings* **2013**, *53*, WC7.
(77) Kim, D. K.; Kim, H. B. *J. Alloys Compd.* **2011**, *509*, 421−425.
(78) Yang, W.; Wu, Z.; Liu, Z.; Pang, A.; Tu, Y.-L.; Feng, Z. C. *Thin Solid Films* **2010**, *519*, 31−36.

DOI: 10.1021/acs.nanolett.5b05124
Nano Lett. 2016, 16, 1925−1932